npj | flexible electronics

Article

Published in partnership with Nanjing Tech University

https://doi.org/10.1038/s41528-026-00567-z

Durable skin-integrated liquid metal-based conductive tattoo for imperceptible and untethered human machine interfaces

Check for updates

Je Hyeong Kim[1,4], Gyeongsuk Park[1,4], Dongeun Kim[1,4], Hanbit Jin[2,4], Jung Rak Choi[2], Minu Kim[1], Seungkyu Lee[1], Minhyung Lee[1], Youngju Son[3], Sangyong Jon[3], Hye Jin Kim[2] ✉ & Steve Park[1] ✉

Electronic tattoos (e-tattoos) hold great potential for next-generation wearable electronics, but their widespread adoption is limited by challenges in electrical conductivity, mechanical durability, and user comfort. In this study, we introduce an Conductive and Durable EGaIn Particle (CDP) ink designed for imperceptible, untethered, and on-palm skin-integrated e-tattoos to overcome these limitations. By leveraging hydrogen bonding between poly(vinyl butyral-co-vinyl alcohol-co-vinyl acetate) (PVB-A) with nanosized silver (Ag) particles and oxide shell of EGaIn-based liquid metal particles, CDP achieves an exceptional initial electrical conductivity of 1.35×10^5 S m^{-1} without post-activation. This formulation facilitates the formation of a stable conductive percolating network while maintaining outstanding mechanical durability and resilience under repeated mechanical stresses, such as rubbing and pinching. These properties arise from the ink's high conductivity even at a low Ag content and the intrinsic robustness of PVB-A with a high density of hydroxyl groups. To demonstrate its functionality, a CDP-based e-tattoo was applied to a human palm as a pressure-sensitive interconnect for human–machine interfaces. This system wirelessly transmitted real-time pressure data from human fingers to a robotic hand, enabling precise grip control. Our findings highlight the potential of CDP ink for advanced, highly durable e-tattoos in interactive and wearable electronic applications.

Traditional textile-based wearable electronics are being utilized in various applications ranging from health monitoring[1–4], metaverse[5], human–machine interface[6], and robotic control[7]. Despite their widespread usage, their bulkiness with rigid components and tethered wires hinders natural human motion and reduces user comfort and convenience. To overcome these drawbacks, ultrathin skin-attachable devices, namely electronic tattoos (e-tattoos), have emerged as a promising alternative. By directly conforming to the skin surface, e-tattoos enable imperceptible integration, intimate skin contact, and stable signal acquisition while preserving natural human motion and tactile sensation[8–10].

Conventional e-tattoos utilize metals such as silver[11] and gold[12–14] to ensure high electrical conductivity. However, poor skin adhesion in regions undergoing frequent and dynamic movement, combined with the inherent rigidity and poor durability of the metals restrict their use under harsh direct-contact mechanical stresses such as grasping and rubbing. Alternatively, 1D/2D materials incorporated into a polymer matrix have been employed as e-tattoos[15–17]. However, these polymer composites have lower electrical conductivity compared to that of metals, restricting their use as interconnects and sensors. Furthermore, achieving sufficient mechanical durability with high conductivity remains challenging due to a trade-off relationship between electrical and mechanical properties[18]. Hydrogels, which exhibit mechanical compliance and stretchability similar to human skin, have also been extensively developed[19–21]. Although hydrogel-based e-tattoos offer enhanced mechanical durability, they pose difficulties in achieving high conductivity, high-resolution patterning, and minimizing device thickness.

[1]Department of Materials Science and Engineering, Korea Advanced Institute of Science and Technology (KAIST), Deajeon, Republic of Korea. [2]Electronics and Telecommunications Research Institute (ETRI), Daejeon, Republic of Korea. [3]Department of Biological Sciences, Korea Advanced Institute of Science and Technology (KAIST), Daejeon, Republic of Korea. [4]These authors contributed equally: Je Hyeong Kim, Gyeongsuk Park, Dongeun Kim, Hanbit Jin.
✉e-mail: nolawara@etri.re.kr; stevepark@kaist.ac.kr

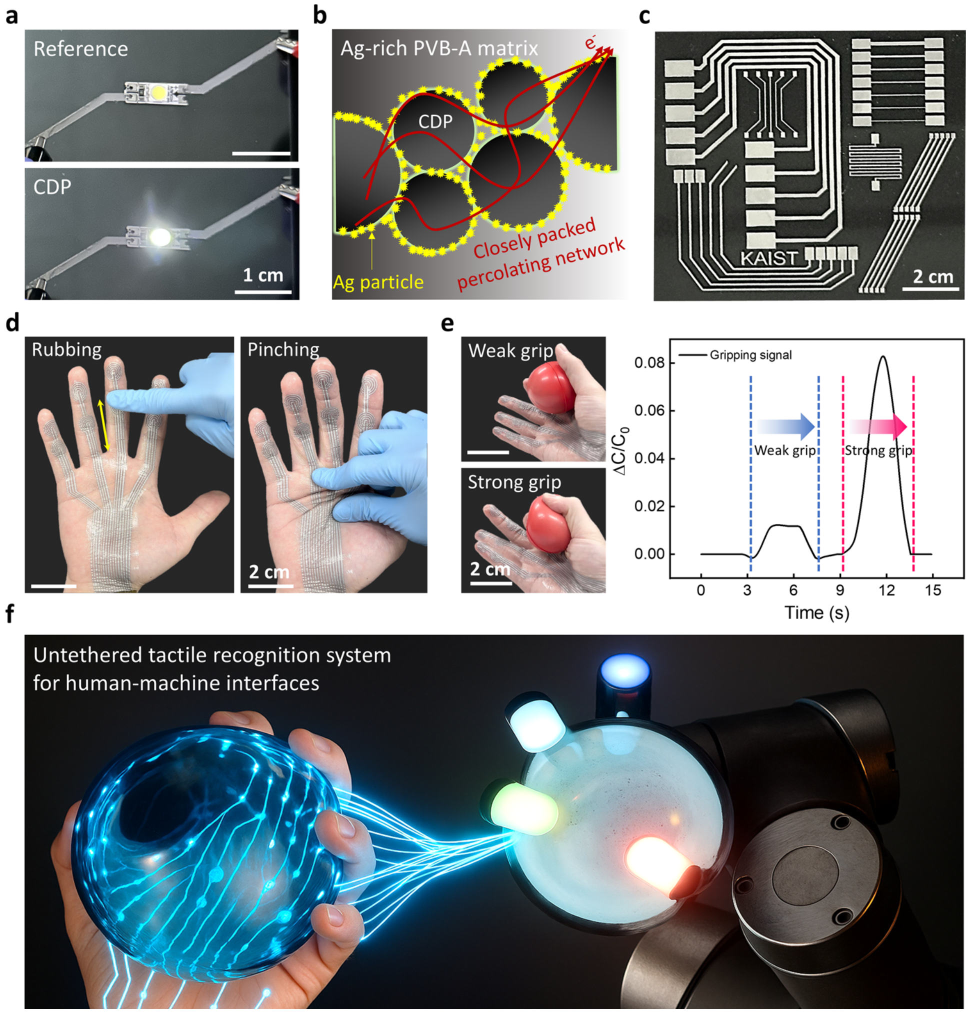

Fig. 1 | Overall concept of conductive and durable EGaIn Particle (CDP). **a** Confirming initially conductive character of CDP through operating a light-emitting diode (LED) compared to the reference. **b** Schematic of a closely packed percolating network of Ag-rich conductive particles. **c** Large-area printability of CDP using the screen printing technique. **d** Photographs of the mechanical stability of CDP attached to a human palm. **e** Demonstration of the e-tattoo distinguishing different grip forces. **f** Schematic of CDP as an e-tattoo on a human palm synchronized with a robotic hand for human–machine interface applications (HMIs).

Eutectic gallium–indium (EGaIn), a type of liquid metal (LM), has been widely explored in stretchable sensors[22–24] and conformal electronics on three-dimensional freeform surfaces[25,26] owing to its high electrical conductivity, deformability, and stretchability, which also make it a promising material for e-tattoo applications. Bulk LM has limited use towards e-tattoos, mainly due to its liquid-like fluidity and high surface tension[27,28]. The use of LM particles (LMP) is a promising alternative as it addresses the above issues[29]. However, since the surrounding oxide shell is insulating, rupturing and merging of the LMPs (i.e., activation) is required to attain conductivity, which reintroduces the drawbacks of bulk LM[30–32]. Several initially conductive e-tattoos have been fabricated by incorporating metallic fillers such as silver flake[33–35], sulfur[36], graphene[37,38], and Pt[39] with EGaIn. However, these designs exhibited low conductivity or poor mechanical properties, highlighting the inherent trade-off between the two properties.

Therefore, despite numerous approaches, there is still an unmet demand for a skin-integrated e-tattoo that is electrically conductive, large-area patternable, and has superior mechanical durability. The latter is particularly critical because the e-tattoo must be mounted on the palmar surface to directly contact external objects during grasping and manipulation, which is essential for tactile-sensing-based human–machine interfaces and robotic control. Furthermore, an untethered wireless system is of high significance to ensure user comfort with no hindrance to natural body motion.

In this work, we present a conductive and durable EGaIn particle (CDP) for on-palm skin-integrated imperceptible and untethered e-tattoo. First, CDP achieved a high initial electrical conductivity of up to 1.35×10^5 S m^{-1} without requiring any post-activation process (Fig. 1a), thus retaining its particulate structure. This high conductivity is attributed to hydrogen bonding between hydroxyl group in poly (vinyl butyral-*co*-vinyl alcohol-*co*-vinyl acetate) (PVB-A) with nanosized-Ag particles and the surface of EGaIn particles, thus resulting in closely packed percolating network of Ag-rich conductive particles (Fig. 1b). CDP can be patterned over a large area (10×10 cm^2) with a line width down to 100 μm, through a simple screen-printing method (Fig. 1c). CDP conformably adheres to the skin and remains firmly attached under repeated rubbing and pinching, while maintaining stable electrical performance under such harsh mechanical deformations (Fig. 1d). With these unprecedented attributes, CDP was attached onto a human palm to serve as a pressure-sensitive e-tattoo and interconnects down to the arm for wireless circuit connection (Fig. 1e). The skin-integrated CDP allows free hand movement while grasping various objects. The pressure data was transmitted wirelessly to a robotic hand to mimic the grasping force, thus opening up the avenue for imperceptible and untethered tactile recognition systems for human–machine interfaces, VR/AR, metaverse, and remote robotic control (Fig. 1f).

Results

Characteristics of initial conductivity and mechanical durability in CDP

To make CDP, we added PVB-A into an ethanol solution containing EGaIn and silver (Ag) flakes, followed by ultrasonication (see details in the "Methods" section). PVB-A was the key component in simultaneously achieving high electrical conductivity and mechanical durability. Sonication breaks up Ag flakes from micro to nano size. Hydroxyl groups on the PVB-A form hydrogen bonds with the Ag nanoparticles (AgNPs), and with the

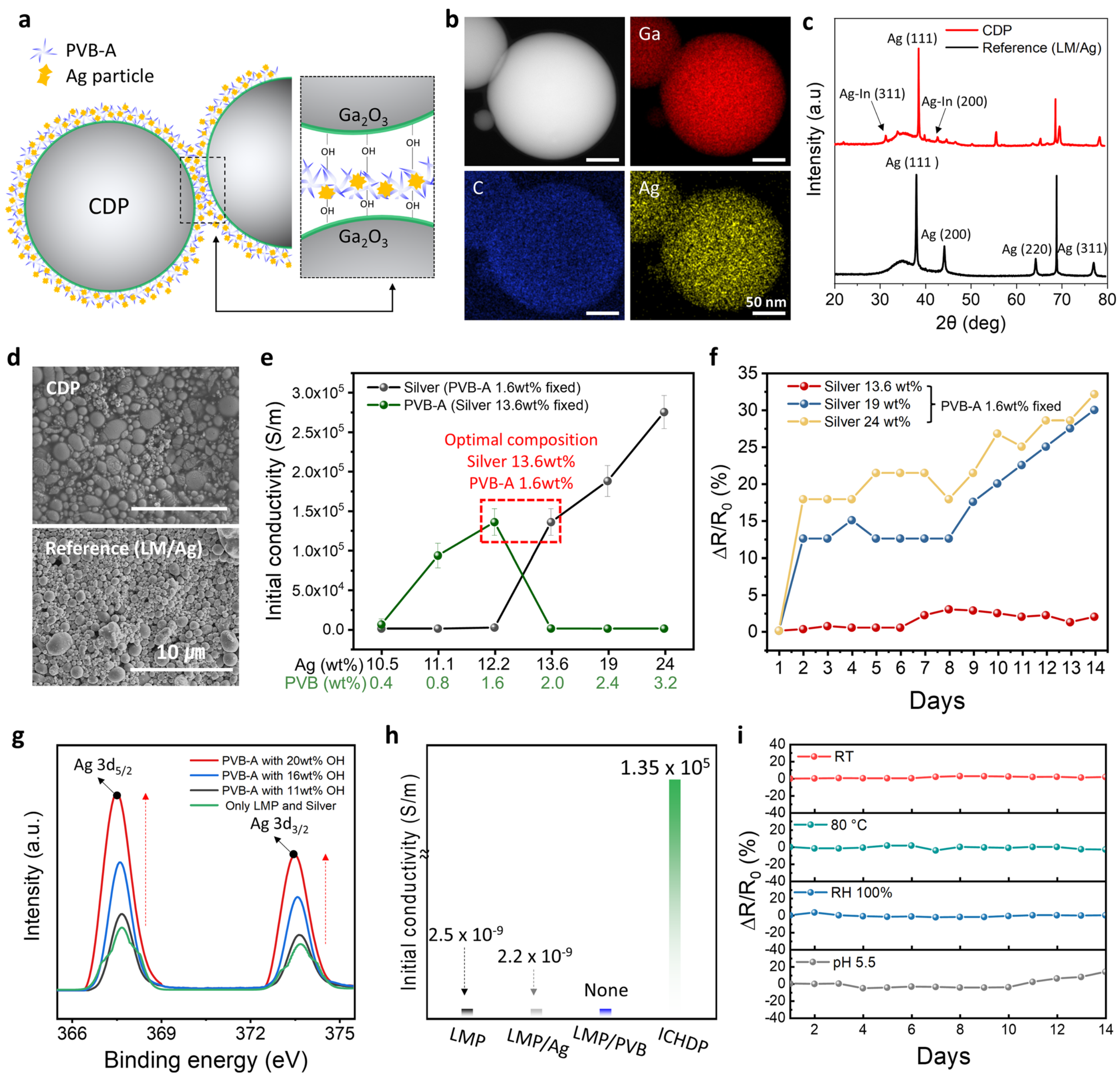

Fig. 2 | Design and characteristics of CDP. **a** Schematic illustration showing the mechanism of the initial conductivity of CDP. **b** TEM EDS images of CDP. **c** X-ray diffraction (XRD) analysis of CDP and reference. **d** SEM images of physically interconnected CDP and separated reference. **e** Initial conductivity depending on the concentration of silver and PVB-A. **f** Long-term electrical resistance degradation in relation to Ag contents at ambient temperature. **g** X-ray photoelectron spectroscopy (XPS) of CDP as the density of the hydroxyl group in PVB-A increased. **h** Initial conductivity varies from particle constituents. **i** Long-term electrical stability in various environments.

LMP surface (Supplementary Note 1)[40–43]. Hence, PVB-A coats the LMPs with Ag NPs and also chemically binds the LMPs together (Fig. 2a).

The presence of Ag on the CDP surface was confirmed by energy-dispersive X-ray spectroscopy (EDS) images from transmission electron microscopy (TEM) analysis (Fig. 2b). Using TEM element profile, the weight fraction of each element on the surface of CDPs and on reference LMPs without PVB-A was measured (Supplementary Fig. 1). The CDP possessed a much higher portion of Ag and indium (In) compared to the reference, verifying the Ag-rich CDP surface. This was further confirmed by X-ray diffraction (XRD) analysis, which also revealed the formation of In/Ag alloy (Fig. 2c). Additionally, CDP exhibits a thinner surface oxide layer compared to that of the reference LMPs, which can additionally contribute to high electrical conduction Supplementary Fig. 2). PVB-A, also functioning as a strong binder between LMPs, generates a stable electrical pathway by closely packing the Ag-rich CDPs, as shown in the scanning electron microscope (SEM) and energy-dispersive X-ray spectroscopy (EDS) images (Fig. 2d and Supplementary Fig. 3).

Optimizing the initial conductivity of CDP requires careful adjustment of Ag flake and PVB-A concentrations. As evident in Fig. 2e green curve, conductivity increases up to 1.6 wt% of PVB-A (Ag concentration fixed at 13.6 wt%), and decreases thereafter, suggesting that excessive PVB-A acts as a barrier for electrical flow. Fixing PVB-A concentration at 1.6 wt%, we varied the Ag concentration (Fig. 2e black curve). Although the conductivity continuously increases with more Ag added, the long-term electrical stability is compromised as seen in Fig. 2f. After 2 weeks, Ag concentrations of 19 and 24 wt% resulted in a drastic resistance increase from the initial state, which is attributed to oxidation of Ag particles that are insufficiently bonded to PVB-A. Consistently, these Ag-rich compositions also exhibited poor

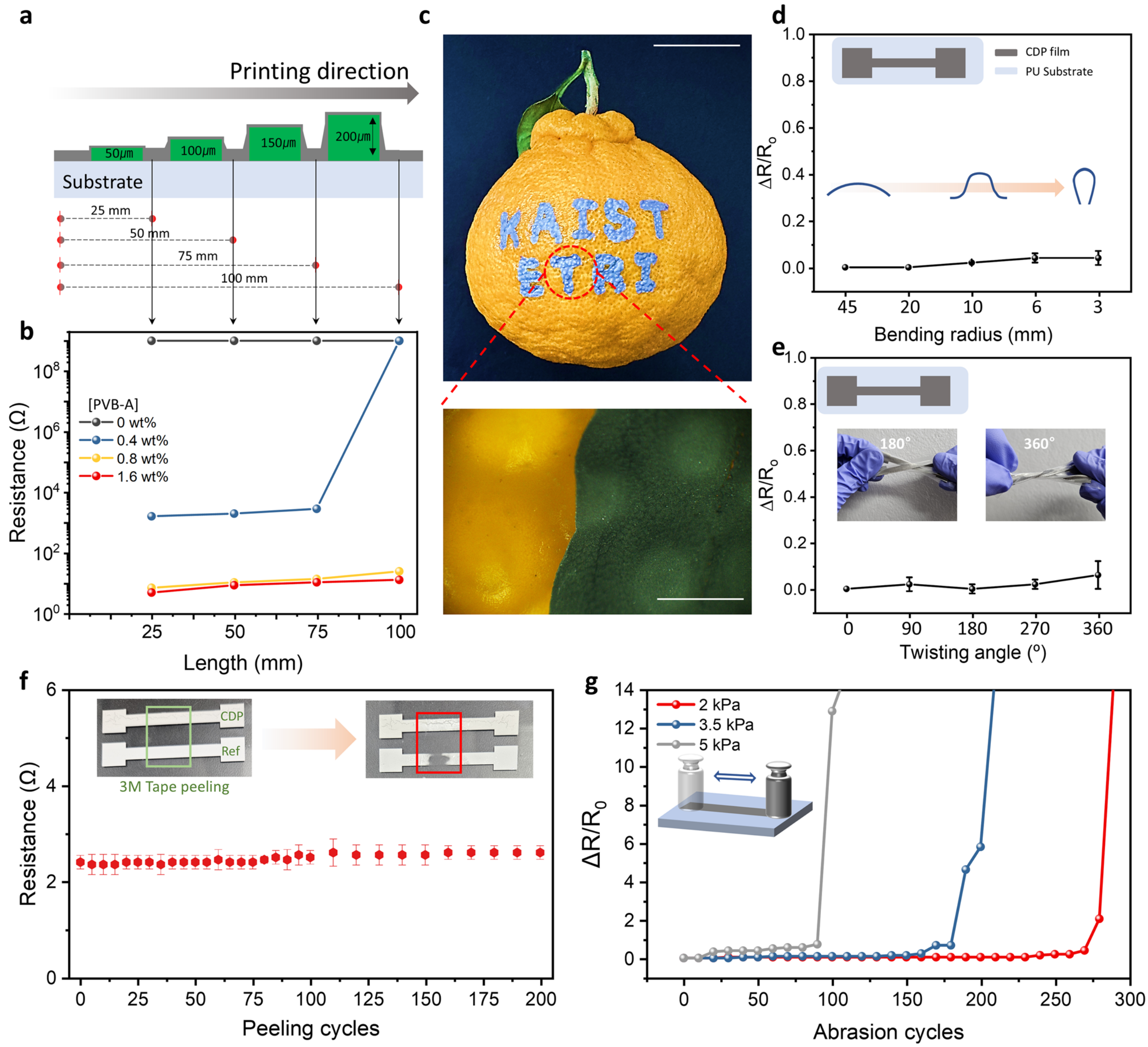

Fig. 3 | Conformal coating and mechanical durability of CDP. **a** Schematic of screen printing over obstacles with height ranging from 50 to 200 μm. **b** The effect of the PVB-A concentration on resistance with length as it crosses over obstacles. **c** Photograph of an orange with alphabet letters drawn on its surface using brush painting (top). OM image showing a magnified view of the surface (bottom). **d** Change in resistance under bending. **e** Change in resistance under twisting. **f** Peel-off cycle test for verifying mechanical durability. **g** Abrasion cycle test for verifying mechanical robustness.

mechanical durability during peeling and rubbing tests (Supplementary Fig. 4), further indicating inadequate particle–polymer bonding. In contrast, an optimal Ag concentration of 13.6 wt% stably maintained its resistance and showed high mechanical durability (Fig. 2f and Supplementary Fig. 4) owing to effective integration of Ag particles within the PVB-A-mediated network. Therefore, the optimal composition of CDP was set at 13.6 wt% Ag and 1.6 wt% PVB-A.

The amount of hydroxyl functional group in PVB-A affects the initial conductivity of CDP, as it changes the number of hydrogen bonds. X-ray photoelectron spectroscopy (XPS) in Fig. 2g exhibited highly enhanced Ag intensity in CDP as the density of the hydroxyl group in PVB-A increased. As shown in Supplementary Figs. 5 and 6, CDP with the higher density of hydroxyl groups presented higher initial conductivity, along with enhanced wettability by lowering the contact angle. The optimized CDP achieved an initial conductivity of 1.35×10^5 S m^{-1} (Fig. 2h). To further assess CDP's electrical stability, we monitored long-term resistance change under various environmental conditions (i.e., RT, 80 °C, RH 100%, and pH 5.5). As shown in Fig. 2i, CDP retains its initial resistance for 2 weeks, verifying its usability across diverse conditions.

Conformal coating and mechanical durability of CDP

In addition to electrical conductivity, the e-tattoo is required to seamlessly cover rough, uneven regions and wrinkles of human skin. To confirm its ability to overcome variations in surface elevation, vertically raised obstacles with heights ranging from 50 to 200 μm were arranged with 50 μm intervals. Applying the screen-printing method, CDP with varying PVB-A content traversed the obstacles, as depicted in Fig. 3a.

As seen in Fig. 3b, a sample without PVB-A was nearly electrically insulating, while a sample composed of 0.4 wt% PVB-A attained electrical conductivity but failed to maintain stable electrical connections over obstacles exceeding a height of 200 μm. Although 0.8 wt% of PVB-A succeeded in establishing an electrical pathway over all obstacles, it showed insufficient electrical stability due to the low viscosity and weak bonding intensity between CDP particles (Supplementary Fig. 7). On the contrary, CDP with 1.6 wt% PVB-A presented the most stable conductivity and an ideal resistance change as the length increased, even when encountering progressively taller obstacles. The optical image in Fig. 3c proves conformal coating of CDP, seamlessly being painted on the bumpy and curved surface of an orange. Therefore, the concentration of PVB-A was found to be critical not only for achieving high initial conductivity (as mentioned in Fig. 2e) but also for ensuring continuous electrical connectivity under high surface roughness.

Next, the mechanical stability of CDP was evaluated through bending, twisting, peeling, and abrasion tests. For bending and twisting tests, polyurethane (PU) was selected as a flexible substrate, onto which CDP was screen-printed using a line-patterned mask. While the sample was gradually subjected to severe bending and twisting (with a bending radius reduced to 3 mm and a twisting angle increased to 360°, respectively), a change in resistance was monitored. Remarkably, CDP exhibited minimal resistance change under both bending and twisting conditions (Fig. 3d and e). In addition, CDP maintained stable electrical resistance under 20% tensile strain over 7000 consecutive stretching cycles, demonstrating its mechanical robustness under repeated deformation (Supplementary Fig. 8).

Furthermore, a peeling test was conducted using 3M tape, where the tape was repeatedly applied and removed from a patterned CDP sample under constant pressure and speed. The reference sample without PVB-A was completely removed after 30 peeling cycles, whereas CDP maintained its initial resistance even after 200 peeling cycles on Polyurethane (Fig. 3f), as well as on PDMS and SEBS substrates (Supplementary Fig. 9). In addition to resistance to peeling, the ability of an e-tattoo to endure intensive external forces, such as abrasion, is crucial for applications involving repeated physical contact. As shown in Fig. 3g, CDP maintained electrical stability under pressures of 2, 3.5, and 5 kPa for up to 250, 180, and 90 abrasion cycles, respectively. This exceptional durability underscores its suitability for practical use under harsh conditions.

The above results verify that our LMPs uniquely possess both high electrical conductivity and mechanical durability, thus making it suitable as a skin-integrated e-tattoo that can be used under harsh mechanical stresses. Such a dual property can firstly be attributed to the property of PVB-A. PVB has been known to have high mechanical strength, impact resistance, durability, and adhesiveness[44]. However, since PVB is an insulating polymer, its usage would lower the electrical conductivity of LMPs. In this work, by utilizing hydrogen bonding via high-density hydroxyl groups in PVB-A[45,46] with Ag and LMPs, high electrical conductivity was maintained by forming a percolating network of Ag-coated LMPs. The second reason for the dual property originates from low conductive filler (i.e., Ag) content. Previous literature indicates that with increasing conductive filler content, the mechanical property of the LMPs is compromised to become brittle, thus making it susceptible to damage under external stimuli[47]. On the other hand, since our system achieves high electrical conductivity even at low Ag content, the deformable property of the LMPs can be maintained.

Pressure-sensitive CDP electronic tattoo (e-tattoo) and its biomedical application

Quantifying and distinguishing pressure exerted on the fingers is a significant challenge, primarily due to the dynamic and irregular deformation of human skin under pressure. Although pressure-sensing gloves have been developed to measure pressure, their bulky and rigid components and wires often hinder natural hand movements, cause user discomfort, and interfere with the tactile sensibility of the user. The CDP e-tattoo provides a solution by applying a skin-integrated e-tattoo directly on the palm of the hand for pressure sensing. This has not yet been demonstrated previously, likely due to the lack of e-tattoo material that simultaneously has sufficient mechanical durability, high conductivity, and large area patternability (Supplementary Table 1 and Supplementary Fig. 10).

The patterning of the e-tattoo was achieved using screen printing, a simple and scalable fabrication process (detailed in the "Methods" section). As illustrated in Fig. 4a, the skin-integrated, pressure-sensitive CDP e-tattoo featuring a circular interdigitated electrode (IDE) pattern was designed to monitor capacitance changes in response to applied pressure, while maintaining mechanical compliance and intimate conformal contact with the skin (Supplementary Fig. 11). When pressure is applied, the distance between the circular IDE patterns on the finger changes due to skin deformation, resulting in a measurable capacitance variation (Supplementary Fig. 12). In contrast, other motions such as finger bending or curvature induce only negligible capacitance changes, confirming that the IDE sensor predominantly responds to pressure-induced stimuli (Supplementary Fig. 13).To optimize the pressure-sensitive IDE pattern, capacitance changes were measured for line gaps of 1000, 700, and 400 μm on an Ecoflex substrate, which has elastic modulus comparable to that of a human finger (Supplementary Fig. 14). The 400 μm gap caused crumpling and shorting, compromising stability. The 1000 μm gap was too wide to cause geometrical changes upon pressure, resulting in low sensitivity. The 700 μm gap provided the most stable and sensitive response. At this spacing, capacitance change of up to 10% over a pressure range of 0–25 kPa was achieved, with cyclic consistency. Therefore, the final IDE design was selected as a circular pattern with a diameter of 15 mm and a line spacing of 700 μm (Fig. 4b).

After optimizing the IDE pattern, the performance of the pressure-sensing e-tattoo was evaluated. The IDE-based CDP e-tattoo exhibited a stable and distinguishable capacitance response over the pressure range of 0–25 kPa, enabling clear differentiation of applied pressure levels (Fig. 4c). The sensor showed a linear response in the low-pressure regime (≈0.6–1.8 kPa) with a sensitivity of ~0.015 kPa^{-1} ($R^2 = 0.995$). In addition, when pressure was increased from 0 to 5 N in 0.1 N increments, the capacitance change was consistently distinguishable across all regions, demonstrating high precision (Fig. 4d). Under repetitive loading–unloading cycles at 1 N, the sensor maintained a stable capacitance variation, confirming the high reliability and mechanical robustness of our CDP e-tattoo (Fig. 4e). The response time was measured to be 50 ms, indicating fast and efficient sensing behavior (Supplementary Fig. 15).

To further confirm the high mechanical durability of the e-tattoos, we applied various mechanical stimuli to the e-tattoo adhered on human palm up to 200 cycles. The CDP e-tattoo exhibited minimal changes in resistance even under repeated physical stimuli such as poking, pinching and rubbing, as shown in Fig. 4f. In addition, the e-tattoo exhibited a stable capacitance response during 4 h of continuous wear under simulated sweating and elevated temperature conditions, and further maintained negligible variation over a 12 h continuous wear test (Supplementary Fig. 16). These results validate the reliable skin adhesion and robustness of the e-tattoo, indicating that it can remain attached under harsh external deformations (Supplementary Video 1) and is suitable for on-palm, direct contact-based human–machine-interfacing applications.

The optimized CDP e-tattoo was further developed into an 8-channel system capable of monitoring pressure at two locations on each of the four fingers (excluding the thumb), and the capacitance changes of each channel was measured during gripping task (Supplementary Fig. 17). When the thumb and index finger grasped a ball, only channels 7 and 8, corresponding to the index finger, exhibited capacitance change (Fig. 4g, left). The CDP e-tattoo was also shown to track the intensity of grip pressure in real time (Supplementary Fig. 18). As more fingers were involved in grasping, the corresponding channels responded with a signal change, as depicted in Fig. 4g, middle and right. These results confirm the precise spatiotemporal and pressure level reading capability of the CDP e-tattoo. Its exceptional durability ensures consistent performance during routine everyday use, highlighting its potential as a skin-integrated sensing system designed to reliably capture and process tactile and biomechanical signal imperceptibly, while allowing natural free-motion and ensuring user comfort. Moreover, the e-tattoo shows no adverse effects on the skin even after prolonged wear (Supplementary Fig. 19).

Apart from an on-palm pressure-detecting application, our skin-integrated CDP e-tattoo is also capable of measuring physiological signals such as electrocardiogram (ECG) and electromyogram (EMG). Our CDP e-tattoo exhibited low impedance compared to the commercial Ag/AgCl electrode under the same coverage area (Supplementary Fig. 20).

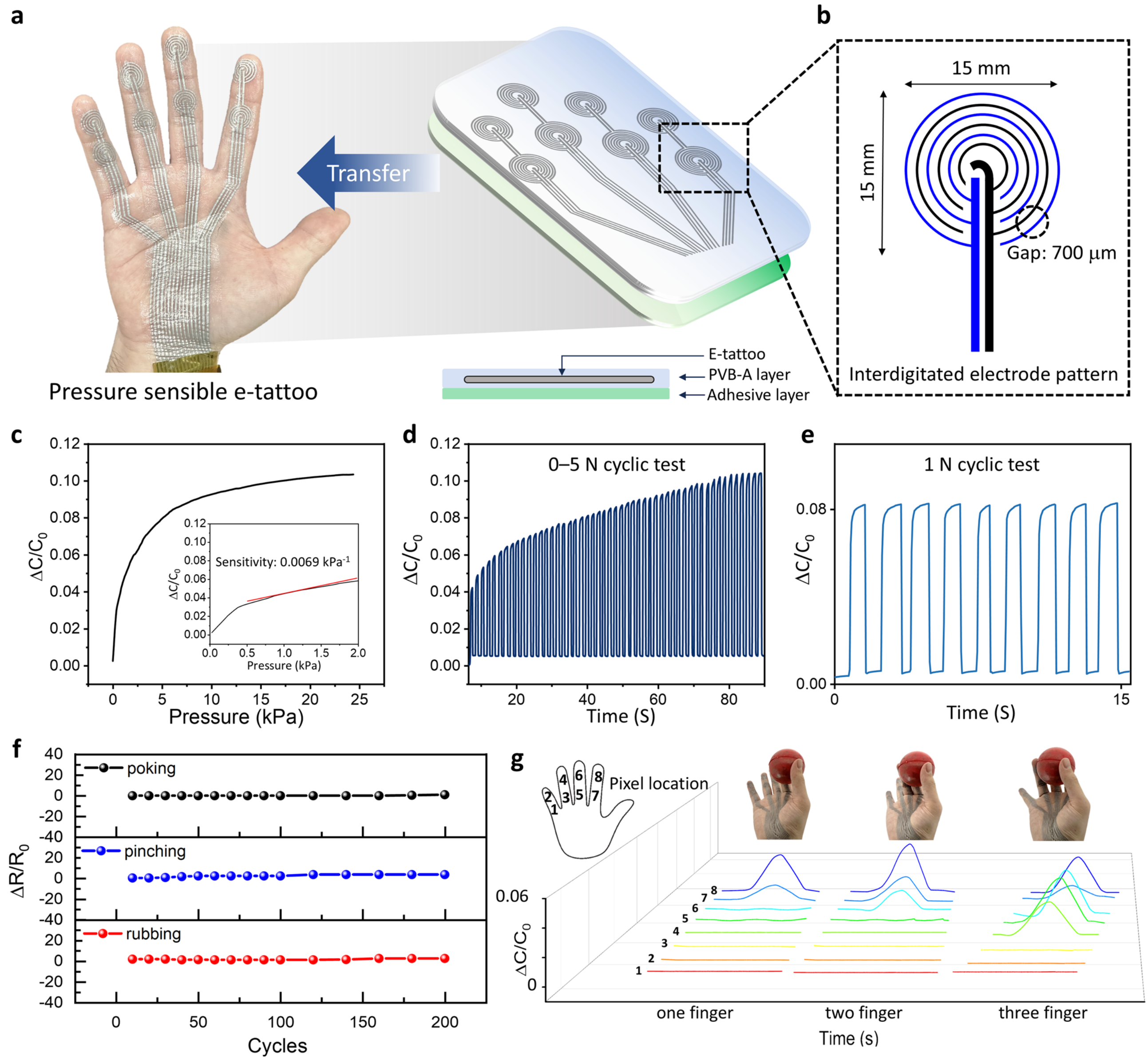

Fig. 4 | Pressure-sensitive CDP electronic tattoo (e-tattoo). **a** Real image and schematic of an 8-pixel CDP e-tattoo attached to the palm. **b** Design of IDE pattern. **c** Change in capacitance of CDP within 0–25 kPa pressure range. Sensitivity of CDP (inset). **d** Capacitance variation of the e-tattoo under gradually increasing pressure from 0 to 50 N with 0.1 N increments. **e** Cyclic test of the e-tattoo under repeated loading–unloading at 1 N, showing stable and repeatable capacitance response. **f** Change in resistance under various mechanical stimuli. **g** Selective pressure-sensing ability of CDP. Change in the capacitance of pixels was measured with an increasing number of grasping fingers.

Supplementary Fig. 21a depicts the measurement setup for EMG and ECG sensing. The e-tattoo successfully detected clear ECG peaks of heart rhythms (Supplementary Fig. 21b) and accurately captured EMG signals associated with forearm movements, showing comparable performance to the Ag/AgCl electrode (Supplementary Fig. 22). Since the CDP e-tattoo conformally adheres to the skin with a thickness of only a few micrometers, it can mitigate signal artifacts arising from external mechanical stress. As depicted in Supplementary Fig. 23, the Ag/AgCl electrode presented severe signal distortion and fluctuation under torsion; however, the CDP e-tattoo exhibited improved signal stability under such mechanical stimulus. These demonstrations primarily highlight the feasibility of physiological signal acquisition using the CDP e-tattoo, confirming that the proposed material system can operate as a practical on-skin electrode under typical measurement conditions. In addition to its reliable electrode characteristics, it has demonstrated biocompatibility, as confirmed by epidermal cell viability in phosphate-buffered saline solution (Supplementary Fig. 24).

Human–machine interface (HMI) application

Figure 5a depicts the human–machine interface (HMI) system where pressure data from the CDP e-tattoo on human fingers is used to wirelessly control the grip intensity of a robot hand. The fingers of the robot hand, equipped with pressure sensors, visually indicate the applied pressure through LED color changes: blue for no pressure, transitioning to teal, green, yellow, and red as pressure intensifies. In the absence of pressure, the robot fingers remain idle, indicating that no objects are being grasped by a human hand. The pressure-sensing interdigitated CDP electrode is extended from the fingers to the wrist and electrically connected to the wireless module via an anisotropic conductive film (ACF), as illustrated in Fig. 5b and Supplementary Fig. 25. Distinct from conventional HMI systems that primarily rely on strain or EMG sensors for motion-based hand replication, our e-tattoo enables direct force sensing and feedback-regulated grasping (Supplementary Table 2). The mechanism of this wireless system is detailed in Fig. 5c, which presents a block diagram depicting how the transmitted

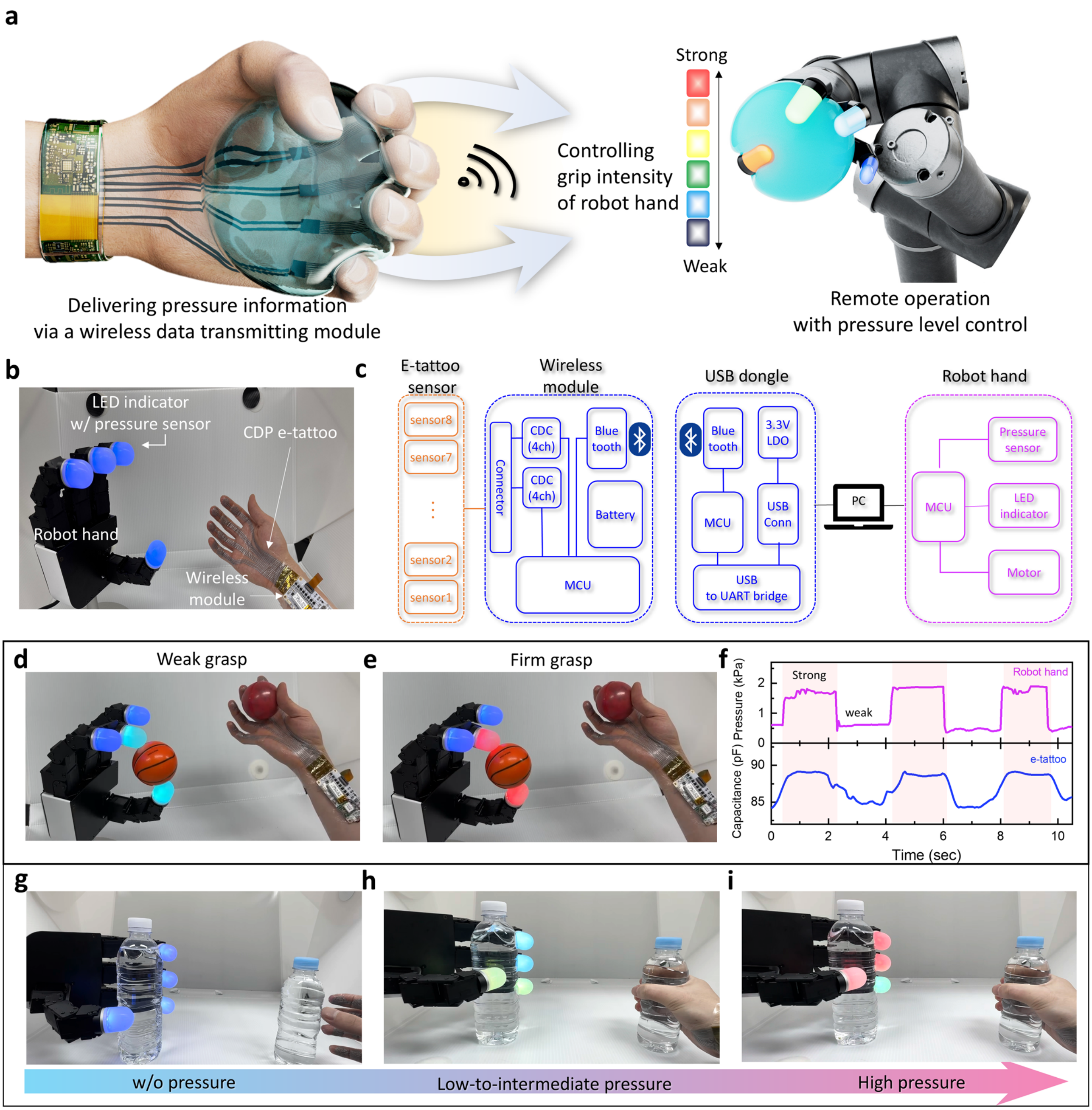

Fig. 5 | A demonstration of robot hand control using a wireless CDP e-tattoo. **a** illustration of robot hand control demonstration using a wireless e-tattoo on a human palm. **b** Image of the robot hand control system. The system consists of a robot hand equipped with an LED indicator and a pressure sensor. It is wirelessly paired with the pressure-sensitive e-tattoo and a wireless module on the wrist. **c** System block diagram of a robot hand control system using an E-tattoo. **d** and **e** Image of a robot hand grasping a sponge ball with weak and strong forces, synchronized with a human hand. **f** Acquired sensor data from the e-tattoo and robot hand while grasping a sponge ball with weak and strong forces. **g**–**i** Image of robot hand grasping a water bottle with low, mid, and high pressure, synchronized with a human hand.

pressure information from the e-tattoo is used to wirelessly control the grip intensity of the robot hand.

Specifically, in this wireless system, a capacitance-to-digital converter monitors the tattoo's capacitance, with data wirelessly transmitted to a PC via Bluetooth. The robotic hand's grasping force was controlled by pre-defined thresholds based on the tattoo's capacitance data. Initial capacitance values were calibrated to account for environmental factors and hand positioning. As pressure was applied, real-time capacitance changes were compared with these thresholds, allowing the robotic hand to adjust its grip strength accordingly. Light pressure triggered a gentle grasp, while higher capacitance values resulted in a firmer grip, ensuring precise and adaptive object handling without excessive force.

The robotic hand successfully grasped a sponge ball with both weak and strong forces, showing fingertip color changes synchronized with grip intensity (Fig. 5d, e, and Supplementary Video 2). Light pressure changed the fingertip color from blue to teal, while a firm grasp shifted it to yellow or red, corresponding to the capacitance data from the tattoo and robotic fingertips during sponge ball manipulation (Fig. 5f). The CDP e-tattoo also identified pressure levels applied by individual human fingers, enabling the robotic arm to replicate grasping motions with corresponding force. It accurately distinguished between no pressure and high pressure, repeatedly performing synchronized grasp-and-release maneuvers with a water bottle, facilitating precise teleoperation (Fig. 5g–i, and Supplementary Video 3). Therefore, this pressure-adaptive HMI system regulates grip intensity while enabling visualization of pressure, thus offering fine-tuned remote robotic control for diverse applications.

Discussion

In this study, we developed a conductive and durable EGaIn particle (CDP) that overcomes the limitations of traditional e-tattoos with poor conductivity and/or mechanical durability. The high initial conductivity (1.35×10^5 S m^{-1}) (i.e., without the need for activation) can be attributed to hydrogen bonding between PVB-A with Ag and EGaIn oxide shell that generates an Ag-rich surface layer and close packs the LMPs to form a conductive percolating network. The high mechanical durability can be ascribed to the low Ag content, along with the intrinsic mechanical durability of PVB-A. As a proof-of-concept, the CDP was conformably attached to an entire palm to detect and classify pressure variations at various positions. The dynamic pressure from the finger is wirelessly translated into robotic actions, highlighting its potential for imperceptible and untethered human–machine interface (HMI) applications. CDP holds significant promise for applications in healthcare monitoring, robotics, human–machine interaction, and next-generation wearable electronics, where user comfort and non-hinderance to natural human motion are of high importance. Future research may focus on directly bonding and integrating the proposed e-tattoo with other smart materials and electronic components to enable additional sensing functionalities and fully skin-integrated systems without the need for external circuit connections. Such advances could facilitate high-fidelity, pressure- and strain-aware human–machine interfaces, including applications in robotic manipulation, teleoperation, surgical robotics, and immersive VR/AR systems, while eliminating bulky wearable accessories. We believe that our work provides a foundation for seamless skin-integrated interfaces that bridge humans with next-generation electronic and robotic platforms.

Methods

Materials

All chemicals used in this study were utilized without further purification unless otherwise stated. Eutectic gallium indium (EGaIn) was sourced from Defense & Engineering (DNE) Co., Ltd. Poly(vinyl butyral)-*co*-(vinyl alcohol)-*co*-(vinyl acetate) (PVB-A), dibutyl sebacate (≥97.0%), and ethanol (99.8%) were obtained from Sigma-Aldrich. Silver flakes (Ag flakes) were procured from DAE JOO Electronics Materials Co., Ltd.

Preparation of CDP Ink

For the preparation of the stretchable PVB-A solution, 2.4 g of PVB-A and 2.4 g of dibutyl sebacate were dissolved in 60 mL of ethanol using mechanical stirring at 50 °C for 24 h to achieve a uniform mixture. To prepare the CDP ink, 1 g of Ag flakes was dispersed in 2.607 g of the prepared PVB-A solution via tip sonication (VC-505, Sonics & Materials, 3 mm microtip) at 30% amplitude for 10 min. The ink was then prepared by combining 0.6 mL of EGaIn with the Ag-dispersed PVB solution in a 10 mL vial, followed by further sonication with the same tip sonicator at 30% amplitude for 20 min. This process yielded the conductive and durable EGaIn particle ink.

Fabrication of CDP e-tattoo

To realize sophisticated interconnects and IDE patterns on the palm, we introduced a water-soluble PVA film as a substrate. The patterned CDP e-tattoo was then encapsulated by PVB-A layers to ensure electrical and mechanical reliability before being transferred to the palm. First, a stencil mask with a pre-designed pattern in AutoCAD was fabricated using a UV laser cutter (MD-U1000C, Keyence) on thermal release tape (RP70N5, T&A Co., Ltd.). To ensure a conformal fit, the mask was applied to a pre-cleaned PVA film. The CDP ink was then patterned onto the PVA substrate using a screen-printing technique. After patterning, the mask was removed by applying heat at 80 °C for 30 min to facilitate easy detachment. PVB-A encapsulation layer was coated over the patterned tattoo to cover the entire surface for flexibility and durability. An adhesive layer was then attached to the top of the PVB-A layer. The assembly was flipped, and the PVA film was completely removed using water to reveal the tattoo pattern. Finally, a second PVB-A layer was applied to the tattoo, completing the encapsulation and enhancing mechanical robustness.

Characterization

XPS analysis (Axis-Supra, Kratos) and XRD analysis (SmartLab, RIGAKU) were performed to chemically characterize CDPs. Additionally, SEM (SU4800, Hitachi) was used to examine the morphology and the thickness (cross-sectional SEM) of the CDP electrode. The sample for measuring the thickness of the electrode was printed on a Si wafer and treated in liquid nitrogen for 1 min. TEM and STEM specimens for the CDP and reference sample were prepared by lifting out via ion-beam milling in a focused ion-beam system (Helios Nanolab 450 F1, FEI). TEM and HAADF-STEM images were acquired using a transmission electron microscope (Talos F200X, FEI) at 200 kV.

Electrical characterization

The electrical resistance of the CDP films and impedance between skin and electrodes were measured using an LCR meter (4284A, HP). Initial conductivity (i.e., electrical conductivity) was evaluated through a four-terminal measurement technique, with gold electrodes placed 1 mm apart on a glass substrate. The thickness of the CDP films was determined using SEM cross-sectional images, with an average thickness of 10 μm calculated from five samples. The electrical conductivity was calculated using the following equation: (1) $\sigma = \frac{\ln 2}{\pi}\left(\frac{1}{Rt}\right) \approx \frac{1}{4.5324}\left(\frac{1}{Rt}\right)$. The compliance and cyclic mechanical performance of the e-tattoo were characterized using an LCR meter, a force gauge (maximum force: 50 N, Mark-10), and a motorized test stand (Mark-10).

Physiological sensing application

EMG and ECG signals were measured with commercial wireless equipment for electro-physiological signal measurement (UC-E6, BITalino). For accurate comparison, a commercial Ag/AgCl gel-type electrode (monitoring electrode 2223H, 3M) was used as the reference and counter electrode in all electro-physiological signal measurements. The performance of the CDP electrode and the commercial Ag/AgCl gel-type electrode as the working electrode was compared. The CDP electrode was directly printed on human skin, and the area of the printed CDP electrode was the same as that of the commercial electrode.

Pressure-sensitive CDP e-tattoo demonstration

The experimental demonstration involved two types of pressure-sensing parts: a pressure-sensitive e-tattoo attached to the human hand and a tactile sensor embedded in the robotic hand. E-tattoo and wireless module are bonding with ACF film (3M *Z*-Axis Conductive Tape 9703). E-tattoo pressure sensors were placed on the index, middle, ring, and little fingers of the human hand. For robotic control, only the index, middle, and ring finger signals were used, as the robotic hand does not include the little finger. The robotic thumb was configured as a passive supporting element; therefore, no sensor was placed on the human thumb. The pressure signal from the middle finger was mapped to a grasp-force scaling parameter to enable continuous modulation of robotic grasping force. The capacitive sensing data, captured from the human hand, was measured by a capacitance-to-digital converter chip (FDC2214, Texas Instruments) and transmitted wirelessly via a Bluetooth module (FB155BC, FirmTech) to the control unit with 20 Hz sampling rate. The robotic hand (Allegro Hand V5(4F) Plus, Wonik Robotics) was equipped with a tactile sensor that gradually changed color from blue to red as the applied pressure increased from 0 to 2 kPa. The robotic hand was controlled through the transmission control protocol (TCP) communication integrated into the Allegro Hand software. To ensure precise control, a custom software interface (Visual Studio, Microsoft) was developed to process the incoming pressure data and map it to predefined hand gestures, such as a grasp.

Ethics approval

Experiments on human skin were conducted with the approval of the Korea Advanced Institute of Science and Technology Institutional Review Board (protocol number: KH2024-110), in accordance with the Declaration of Helsinki. All subjects voluntarily participated in the experiments with informed consent.

Data availability

The datasets generated and analyzed during the current study are not publicly available due to the large size of the raw datasets, but are available from the corresponding author on reasonable request.

Received: 20 November 2025; Accepted: 9 March 2026;
Published online: 14 April 2026

References

1. Chortos, A., Liu, J. & Bao, Z. Pursuing prosthetic electronic skin. *Nat. Mater.* **15**, 937–950 (2016).
2. Geissler, D. et al. Embedding textile capacitive sensing into smart wearables as a versatile solution for human motion capturing. *Sci. Rep.* **14**, 15797 (2024).
3. Lee, J. et al. Highly sensitive multifilament fiber strain sensors with ultrabroad sensing range for textile electronics. *ACS Nano* **12**, 4259–4268 (2018).
4. Wu, S., Peng, S., Yu, Y. & Wang, C. H. Strategies for designing stretchable strain sensors and conductors. *Adv. Mater. Technol.* **5**, 1900908 (2020).
5. Kim, K., Yang, H., Lee, J. & Lee, W. G. Metaverse wearables for immersive digital healthcare: a review. *Adv. Sci.* **10**, 2303234 (2023).
6. Jin, H. et al. Highly pixelated, untethered tactile interfaces for an ultra-flexible on-skin telehaptic system. *npj Flex. Electron.* **6**, 16 (2022).
7. Kwon, S. Y. et al. On-skin and tele-haptic application of mechanically decoupled taxel array on dynamically moving and soft surfaces. *npj Flex. Electron.* **6**, 33 (2022).
8. Kim, C. H., Lee, D. H., Youn, J., Lee, H. & Jeong, J. Simple and cost-effective microfabrication of flexible and stretchable electronics for wearable multi-functional electrophysiological monitoring. *Sci. Rep.* **11**, 14823 (2021).
9. Li, H. et al. E-tattoos: toward functional but imperceptible interfacing with human skin. *Chem. Rev.* **124**, 3220–3283 (2024).
10. Won, P. et al. Stretchable and transparent kirigami conductor of nanowire percolation network for electronic skin applications. *Nano Lett.* **19**, 6087–6096 (2019).
11. Choi, S. et al. Highly conductive, stretchable and biocompatible Ag–Au core–sheath nanowire composite for wearable and implantable bioelectronics. *Nat. Nanotechnol.* **13**, 1048–1056 (2018).
12. Ha, T. et al. A chest-laminated ultrathin and stretchable e-tattoo for the measurement of electrocardiogram, seismocardiogram, and cardiac time intervals. *Adv. Sci.* **6**, 1900290 (2019).
13. Wang, Y. et al. Low-cost, μm-thick, tape-free electronic tattoo sensors with minimized motion and sweat artifacts. *npj Flex. Electron.* **2**, 19 (2018).
14. Niu, H. et al. Low-cost, large-area, multifunctional stretchable e-tattoos inspired by dough figurines for wearable human–machine interfaces. *Adv. Mater. Technol.* **7**, 2100907 (2021).
15. Jang, H. et al. Graphene e-tattoos for unobstructive ambulatory electrodermal activity sensing on the palm enabled by heterogeneous serpentine ribbons. *Nat. Commun.* **13**, 6604 (2022).
16. Gogurla, N. & Kim, S. Self-powered and imperceptible electronic tattoos based on silk protein nanofiber and carbon nanotubes for human–machine interfaces. *Adv. Energy Mater.* **11**, 2100801 (2021).
17. Wang, Q. et al. Self-healable multifunctional electronic tattoos based on silk and graphene. *Adv. Funct. Mater.* **29**, 1908695 (2019).
18. Zhang, S. et al. Carbon nanotube/carbon composite fiber with improved strength and electrical conductivity via interface engineering. *Carbon* **144**, 628–638 (2019).
19. Chong, J. et al. Highly conductive tissue-like hydrogel interface through template-directed assembly. *Nat. Commun.* **14**, 2206 (2023).
20. Jin, S., Kim, Y., Son, D. & Shin, M. Tissue adhesive, conductive, and injectable cellulose hydrogel ink for on-skin direct writing of electronics. *Gels* **8**, 336 (2022).
21. Zhuo, S. et al. Reusable free-standing hydrogel electronic tattoo sensors with superior performance. *npj Flex. Electron.* **8**, 35 (2024).
22. Dickey, M. D. Stretchable and soft electronics using liquid metals. *Adv. Mater.* **29**, 1606425 (2017).
23. Seo, H. et al. Self-packaged stretchable printed circuits with ligand-bound liquid metal particles in elastomer. *Nat. Commun.* **16**, 4944 (2025).
24. Kim, K. K. et al. A simplified wearable device powered by a generative EMG network for hand-gesture recognition and gait prediction. *Nat. Sen.* **1**, 12 (2025).
25. Jiayun, C. et al. Printing completely conformal liquid metal circuits on arbitrary curved surfaces via customized conformal mask. *Adv. Eng. Mater.* **26**, 2400220 (2024).
26. Shuo, Z. et al. High-fidelity conformal printing of 3d liquid alloy circuits for soft electronics. *ACS Appl. Mater. Interfaces* **11**, 7148–7156 (2019).
27. Ge, W. et al. Recent progress in eutectic gallium indium (EGaIn): surface modification and applications. *J. Mater. Chem. A* **12**, 657–689 (2024).
28. He, J. et al. Recent development in liquid metal materials. *ChemistryOpen* **10**, 360–372 (2021).
29. Park, G. et al. Divide and conquer: design of gallium-based liquid metal particles for soft and stretchable electronics. *Adv. Funct. Mater.* **34**, 2309660 (2023).
30. Li, F. et al. Ultra-conformable liquid metal particle monolayer on air/water interface for substrate-free e-tattoo. *npj Flex. Electron.* **7**, 9 (2023).
31. Xu, Y. et al. Convergent synthesis of diversified reversible network leads to liquid metal-containing conductive hydrogel adhesives. *Nat. Commun.* **12**, 2407 (2021).
32. Yan, J. et al. Solution processable liquid metal nanodroplets by surface-initiated atom transfer radical polymerization. *Nat. Nanotechnol.* **14**, 684–690 (2019).
33. Zhao, Y. et al. A self-healing electrically conductive organogel composite. *Nat. Electron.* **6**, 206–215 (2023).
34. Zheng, R. et al. A novel conductive core–shell particle based on liquid metal for fabricating real-time self-repairing flexible circuits. *Adv. Funct. Mater.* **30**, 19010524 (2020).
35. Pozarycki, T. A. et al. A flexible and electrically conductive liquid metal adhesive for hybrid electronic integration. *Adv. Funct. Mater.* **34**, 2313567 (2024).
36. Xin, Y. et al. Ultrauniform embedded liquid metal in sulfur polymers for recyclable, conductive, and self-healable materials. *Adv. Funct. Mater.* **29**, 1808989 (2019).
37. Saborio, M. G. et al. Liquid metal droplet and graphene co-fillers for electrically conductive flexible composites. *Small* **16**, 1903753 (2020).
38. Hu, Y. et al. Graphene oxide encapsulating liquid metal to toughen hydrogel. *Adv. Funct. Mater.* **31**, 2106761 (2021).
39. Lee, G. H. et al. A personalized electronic tattoo for healthcare realized by on-the-spot assembly of an intrinsically conductive and durable liquid-metal composite. *Adv. Mater.* **34**, 2204159 (2022).
40. Kim, J.-H., Kim, S., Dickey, M. D., So, J.-H. & Koo, H.-J. Interface of gallium-based liquid metals: oxide skin, wetting, and applications. *Nanoscale Horiz.* **9**, 1099–1119 (2024).
41. Jo, Y. et al. Printable self-activated liquid metal stretchable conductors from polyvinylpyrrolidone-functionalized eutectic gallium

indium composites. *ACS Appl. Mater. Interfaces* **14**, 10747–10757 (2022).
42. Wu, Y. et al. Fabrication and interfacial characteristics of surface modified Ag nanoparticle-based conductive composites. *RSC Adv.* **7**, 29702–29712 (2017).
43. Chou, H. L., Wu, C. M., Lin, F. D. & Rick, J. Interactions between silver nanoparticles and polyvinyl alcohol nanofibers. *AIP Adv.* **4**, 087134 (2014).
44. Matsumoto, T., Yorifuji, M., Sugiyama, Y. & Nishino, T. Butyralization of poly(vinyl alcohol) under supercritical carbon dioxide for a humidity-resistant adhesive to glass substrates. *Polym. J.* **52**, 1349–1356 (2020).
45. Harandi, D., Gonzalez-Benito, J. & Olmos, D. Consolidation of fir wood by poly(vinyl butyral-co-vinyl alcohol-co-vinyl acetate) treatment: study of surface and mechanical characteristics. *Polymers* **12**, 1039 (2020).
46. Samide, A., Merisanu, C., Tutunaru, B. & Iacobescu, G. E. Poly(vinyl butyral-co-vinyl alcohol-co-vinyl acetate) coating performance on copper corrosion in saline environment. *Molecules* **25**, 30439 (2020).
47. Tavakoli, M. et al. 3R electronics: scalable fabrication of resilient, repairable, and recyclable soft-matter electronics. *Adv. Mater.* **34**, 2203266 (2022).

Acknowledgements
This work was supported by the Institute of Information & Communications Technology Planning & Evaluation (IITP) by the Korea Government Ministry of Science and ICT (MSIT) (No. RS-2025-02303658), Korea Evaluation Institute of Industrial Technology (KEIT) grant funded by the Korea government (MOTIE, grant no. RS-2022-00154781, Development of large-area wafer-level flexible/stretchable hybrid sensor platform technology for formfactor-free highly integrated convergence sensor), and Institute of Information & communications Technology Planning & Evaluation (IITP) grant funded by the Korea government (MSIT) (No. RS-2022-II220025, Development of soft-suit technology to support human motor ability).

Author contributions
J. H. Kim, G. Park, D. Kim, and H. Jin conceived the overall idea and established the project framework. G. Park and D. Kim formulated the ink system and carried out the chemical analyses. H. Jin and J. H. Kim performed the electrical measurements and processed the resulting data. G. Park, D. Kim, and M. Lee designed the IDE structures. J. R. Choi, M. Kim, and S. Lee developed and implemented the human–machine interface demonstrations. H. Jin built the wireless robotic control platform. Y. Son and S. Jon evaluated the biocompatibility. H. J. Kim and S. Park supervised and coordinated all stages of the research. G. Park drafted the initial manuscript, and J. H. Kim, D. Kim, and H. Jin contributed to manuscript revision. All authors reviewed and commented on the final manuscript.

Competing interests
The authors declare no competing interests.

Additional information
Supplementary information The online version contains supplementary material available at https://doi.org/10.1038/s41528-026-00567-z.

Correspondence and requests for materials should be addressed to Hye Jin Kim or Steve Park.